Journal of Applied Electrochemistry (2007) 37:103–110
DOI 10.1007/s10800-006-9207-y

Investigation of the response of separate electrodes in a polymer electrolyte membrane fuel cell without reference electrode

MATHIEU BOILLOT[1], CAROLINE BONNET[1,*], SOPHIE DIDIERJEAN[2] and FRANÇOIS LAPICQUE[1]
[1]*Laboratoire des Sciences du Génie Chimique, CNRS-ENSIC-INPL, 1 rue Grandville, BP 20451 54001, Nancy, France*
[2]*Laboratoire d'Energétique et de Mécanique Théorique et Appliquée, INPL-UHP, 2 avenue de la Forêt de Haye, 54504, Vandœuvre les Nancy, France*
*(*author for correspondence, tel.: + 33-383-175-119, fax: + 33-383-322-975, e-mail: bonnet@ensic.inpl-nancy.fr)*

Received 14 February 2006; accepted in revised form 20 June 2006

Key words: electrochemical investigation, hydrogen oxidation, impedance spectroscopy, oxygen reduction, PEM Fuel cells

Abstract

The paper presents electrochemical measurements carried out in a PEMFC with a view to determining the separate kinetics of the electrode reactions. For this purpose, the separate response of one electrode (anode or cathode) was magnified by dilution of the reacting gas, respectively hydrogen and oxygen, and comparison of the experimental data in the form of steady voltage-current variations and impedance spectra. Experiments were carried out at 60 °C and ambient pressure. Water management was thoroughly controlled so that the gases leaving the cell had the same relative humidity in all experiments of one series. Hydrogen oxidation, although rapid, corresponds to overpotentials up to 50 mV at high dilution rates and current densities. Assuming a Tafel–Volmer mechanism, the exchange current density of the anode reaction at the Pt surface is of the order of 1 mA cm^{-2}. The two techniques employed led to Tafel slopes of oxygen reduction ranging from 120 to 150 mV/decade, with an exchange current density near 1 μA cm^{-2}, in good agreement with published data.

Abbreviations

b_T	Tafel coefficient, V/decade
C	concentration, mol m^{-3}
D	diffusion coefficient, m^2 s^{-1}
e	electron
F	Faraday's constant, 96487 C mol^{-1}
I	current, A
i	current density, A m^{-2} or A cm^{-2}
i_L	limiting current density, A m^{-2} or A cm^{-2}
i_0	exchange current density, A m^{-2} or A cm^{-2}
J	specific flux mol m^{-2} s^{-1}
m	partitioning coefficient
n	number of electrons involved
P	pressure, Atm
Q	pseudocapacitance, S cm^{-2} s^{α}
R	gas constant, 8.314 J K^{-1} mol^{-1}
r	specific resistance, Ω cm^2
T	temperature, K
U_{rev}	reversible voltage, V
V	cell voltage, V
Z	impedance, Ω

Greek letters

α	exponent of constant phase element
α	charge transfer coefficient
γ	ration of effective area over geometrical area
δ	layer thickness, m
ε	porosity
η	overpotential, V
∞	bulk conditions

Subscripts

a	anode
c	cathode
CPE	constant phase element
ct	charge transfer
diff	diffusion
eff	effective
L	limiting
N	Nafion
ohm	ohmic
Ox	oxidant
Red	reductant
0	electrode surface
1	gas diffusion electrode
2	electrode structure

1. Introduction

In PEM fuel cells the oxidation of hydrogen is often neglected in comparison to oxygen reduction, because of the slow kinetics of the latter reaction on platinum surfaces. Under such assumptions, the overall impedance response of the cell is therefore attributed to the cathode response. In order to validate this assumption, it is necessary to extract the response of each electrode from the overall electrochemical information. This could be done using a reference electrode in the cell, but its positioning may raise technological issues [1, 2], resulting in inaccurate measurements. More recent investigations led to technological improvements either in the form of a dynamic hydrogen electrode unit [3] or a microsized carbon filament inserted in the membrane [4].

Aside from these developments, the present investigation was aimed at estimating the contributions of separate anode and cathode in a PEMFC. For this purpose, the significance of the anode response was magnified by diluting hydrogen by nitrogen at various ratios. Diluted oxygen -with pure hydrogen at the anode- also allowed similar investigation to be carried out for the cathode part. Operating conditions were thoroughly controlled so that all parameters, in particular water management was kept identical: the difference observed in the impedance spectra and in the voltage-current density variations could then be attributed to the contribution of the electrodes investigated.

2. Experimental section and methods

2.1. *Experimental set-up*

The fuel cell tested was a single cell FC25-01SP from Electrochem, with a geometric area of 25 cm^2. Gases were distributed through the ''column'' pattern of the plate, consisting of 2 mm cubic tiles placed regularly in the plate. The commercial membrane electrode assemblies consist of two electrodes 1 mg/cm^2 Pt with a 20% wt Pt/C ratio, a Nafion® 115 membrane and Toray® carbon paper backings.

Before entering the fuel cell, gases were humidified in laboratory-designed packed columns filled with deionised water. The humidification temperatures at both sides were fixed by thorough control of the dew points of the packed bed columns, which were heated by separate water baths. The cell temperature was efficiently controlled by using Peltier thermoelements fixed on both external plates of the cell. The two gaseous streams leaving the cell were condensed at ambient temperature. The amounts of water in each side of the cell were calculated by weighing the amount of water condensed for times up to three hours, and taking into account the vapour pressure at the ambient temperature.

Electrical measurements were carried out using an Autolab PGSTAT30 (Eco Chemie) potentiostat/galvanostat connected to a current booster BSTR20A (Eco Chemie). Measurements were carried out in two steps:

- the cell voltage was first recorded for time periods from one to three hours, allowing steady state behaviour to be attained;
- impedance spectra were then recorded at the considered current density. The amplitude of the sine perturbation was fixed at 10% of the steady current. Frequencies were scanned from 5 to 10 mHz, with 10 points per decade: frequencies higher than 5 kHz resulted in particular cell responses, probably due to the dynamics of the electrical equipment used.

2.2. *Operating conditions*

The cell temperature was fixed at 60 °C and all experiments were carried out at ambient pressure. The stoichiometric factor of air fed to the anode for investigation of the anode kinetics was fixed at 3, whereas it was at 2 for pure hydrogen for investigation of the cathode response. In addition, at a given nominal current, the global gas flow rate in the working electrode compartment was kept constant, so that the amount of water introduced into the cell was independent of the dilution: for anode response, hydrogen was diluted at 20, 40, 60, 80, and 100% in nitrogen, with respective stoichiometric factors respectively at 2, 4, 6, 8, and 10. Likewise, the oxygen content was 21 (air), 40, 60, 80 and 100% for investigation of the cathode side, with the same stoichiometric factors as for anode investigation. The percentages given above are for dry gases, regardless of the vapour added downstream of the flowmeters.

For anode investigations, the relative humidity of the inlet gases was 63 ± 2% at the cathode, and 83 ± 2% at the anode. The gases leaving the cathode were saturated with water in all cases, with fractions of liquid water on this side at 15 ± 2% at 60 °C. The relative humidity of the anode gas was 95 ± 2% at this temperature.

For cathode investigations, the relative humidity of the inlet gases was 67 ± 2% at the cathode and 90 ± 2% at the anode. Air leaving the cathode was saturated with water, with fractions of liquid water attaining 44 ± 2%. The anode gas was also saturated with water, with liquid mass fraction below 5%.

2.3. *Impedance model*

Kinetic parameters were estimated from impedance spectra using a model for the cell response: this model was established considering the equivalent circuit shown in Figure 1.

The anode response corresponds to the left part of the circuit and should be observed for high frequencies, since the charge transfer resistance is far lower than that of the cathode side. A typical experimental impedance spectrum obtained for high hydrogen dilution is shown in Figure 2.

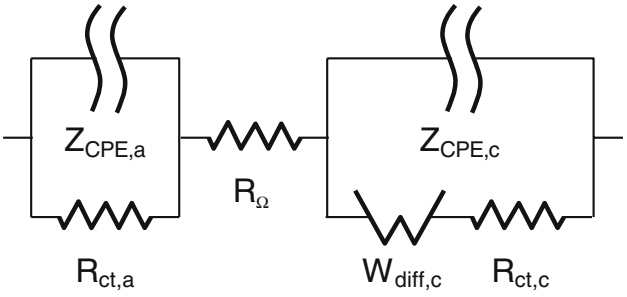

Fig. 1. Electrical equivalent circuit of the cell.

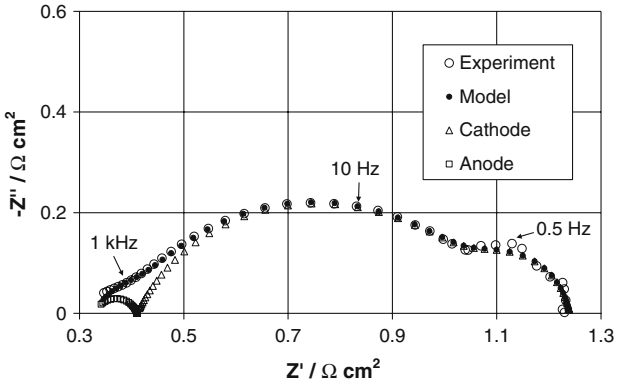

Fig. 2. Typical experimental impedance response and global model with anode and cathode corresponding responses. Current density: 200 mA cm^{-2}. Anode fed with 20% hydrogen diluted in nitrogen.

By comparison with spectra recorded with pure hydrogen, the spectrum shown in Figure 2 has a larger high frequency loop. For all cases, spectra presented three more or less distinct loops, referred to as high, medium and low frequency loops:

- the high-frequency loop was attributed to hydrogen oxidation, as confirmed below;
- the large loop at medium frequency was usually considered to be due to the cathode charge transfer resistance.
- the low-frequency loop has been ascribed to the diffusion of oxygen as shown by Freire and Gonzalez [5], or water as described in [6]. Nevertheless we observed previously [7] that the low frequency loop could result from diffusion of gaseous oxygen in nitrogen. This loop was not discussed in the present paper.

For both electrodes, constant phase elements $Z_{CPE,a}$ and $Z_{CPE,c}$ were considered, with pseudo-capacitances Q_a and Q_c, and exponents α_a and α_c [8]. The model considered involves a large number of parameters: three for the (R_aQ_a) of the anode (following the Boukamp notation of electrical circuits [9]), and five for the $([R_cO_c]Q_c)$ circuit of the cathode, in addition to r_{ohm}. Spectra were interpreted as follows. First the right hand circuit in Figure 1 was considered by fitting the low frequency part of the spectra, in the range 10 mHz–45 Hz. The estimates obtained were then used in the fitting of the high frequency part of the spectrum – over 35 Hz, allowing determination of parameters $r_{ct,a}$, $Q_a$and α_a. The set of parameter values was finally used in fitting the whole experimental spectrum for more accurate determination of the various parameters. The various contributions of the spectra extracted through interpretation of the experimental spectrum are shown in Figure 2. The accuracy in fitting the anodic part is moderate, and it was preferred to fix α_a at 0.8. In addition the values for Q_a and $r_{ct,a}$ are given with an uncertainty in their determination estimated at 30%.

2.4. *Expression of the current density and charge transfer resistance*

Consider the following reversible reaction

$$\mathrm{Ox} + n\ \mathrm{e} \leftrightarrow \mathrm{Red} \tag{1}$$

The Butler–Volmer equation allows expression of the current density as a function of the electrode overpotential η, involving species concentrations at the electrode surface and in the bulk as follows:

$$i(t) = i_0\left[\frac{\mathrm{Red}(0,t)}{\mathrm{Red}(\infty)}\exp\left(\frac{\alpha nF}{RT}\eta(t)\right) - \frac{\mathrm{Ox}(0,t)}{\mathrm{Ox}(\infty)}\exp\left(-\frac{(1-\alpha)nF}{RT}\eta(t)\right)\right] \tag{2}$$

where i_0 is the exchange current density and α the charge transfer coefficient. The charge transfer resistance, r_{ct}, can be derived from the current density:

$$r_{ct} = \left(\frac{\partial\eta}{\partial i}\right) \tag{3}$$

The concentration ratios involved in the above relation depend on the rate of transport from the gas bulk to the electrode surface. Transport phenomena in the fuel cell are the following: (i) transfer from the gas bulk in the pattern of the bipolar plate to the surface of the gas diffusion layer, (ii) transport through the gas diffusion layer (GDL), (iii) diffusion through the carbon material forming the electrode and, finally, diffusion in the thin electrolyte layer (iv). These phenomena were assumed to be one-dimensional processes. Moreover, mass transfer in the bipolar plate was not considered here because of the lack of existing correlations for the "column" pattern considered here.

Transport in the GDL, subscript 1, was assumed to consist of pure diffusion and the effective diffusivity of the gas was estimated using Bruggeman's relation:

$$D_{\mathrm{eff},1} = D\varepsilon_1^{3/2} \tag{4}$$

The porosity ε_1 of the GDL was taken at 0.4 [10]. Due to the average pore size in the structure of carbon electrode (medium 2), Knudsen diffusion was accounted for in estimation of the overall diffusion coefficient, using Chapman–Enskog's relation. Molecular diffusivities were taken from [11] since the published data were obtained at 60 °C. The pore size in the electrode

structure was fixed at 30 nm, and porosity ε_2 at 0.3, as considered in [11, 12]. Finally, diffusion in the electrolyte (subscript N) involves dissolved gases. The partition coefficient, m, was defined as the gas-over-liquid concentration ratio. Calculations were carried out for the case of Nafion 115 with electrode thickness of 50 μm (Table 1), for the actual temperature, and the relative humidity was taken at 75%. Values for diffusivity and solubility of nitrogen and oxygen were those measured by Gode et al. [11]. Table 1 summarises the values of the various dimensions and physicochemical parameters used.

For the conversion of gas, the reactant concentration at the electrode surface, $C(0)$, could then be expressed versus the bulk gas concentration $C(\infty)$ and specific flux J of this species:

$$C(0) = \frac{C(\infty)}{m} - J\left[\frac{\delta_1}{mD_{\text{eff},1}} + \frac{\delta_2}{mD_{\text{eff},2}} + \frac{\delta_N}{\gamma D_N}\right] \tag{5}$$

The coefficient γ is the ratio of the active area of the electrode over its geometrical area. For both electrodes, γ was taken to be 200 [13]. The limiting current density corresponding to total depletion of the reactant at the electrode surface was then deduced:

$$i_L = \frac{nFC(\infty)}{\frac{\delta_1}{D_{\text{eff},1}} + \frac{\delta_2}{D_{\text{eff},2}} + \frac{m\delta_N}{\gamma D_N}} \tag{6}$$

Table 1. Characteristic variables of the membrane electrode assembly used at 60 °C

	Gas diffusion layer	Electrode carbon material	Electrolyte layer in the electrode
Thickness/μm	180	50	0.1
Pore size/μm	20	0.03	–
Porosity ε	0.4	0.3	–
Surface ratio γ			200
H_2 diffusivity/m^2 s^{-1}	2×10^{-5}	3×10^{-6}	7.1×10^{-10}
O_2 diffusivity/m^2 s^{-1}	0.8×10^{-5}	7×10^{-7}	1.7×10^{-10}

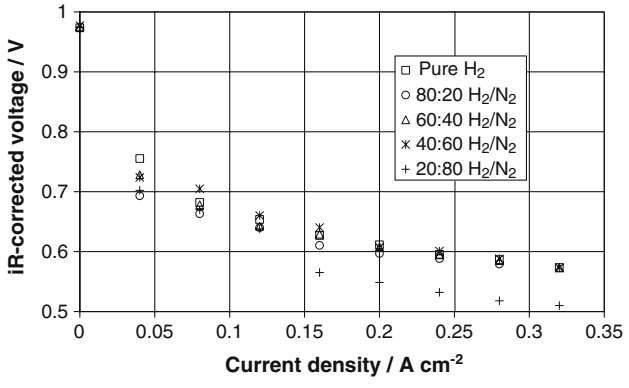

Fig. 3. Cell voltage corrected for ohmic drop, for all hydrogen dilutions.

3. Anodic oxidation of hydrogen

The voltage–current curves corrected for the ohmic drop in the cell are reported in Figure 3 for all hydrogen dilutions.

Because of the moderate partial pressures of the reacting gases, the current density delivered by the single cell was below 0.4 A cm^{-2}. Values for the ohmic resistance were deduced from the impedance spectra and the average value was 0.31 ± 0.02 Ω cm^2. The voltage-current variations with the hydrogen concentration in the gas were of the order of the fluctuations recorded along the runs, of the order of 20 mV. Data obtained at high current density and with 20% H_2 are significantly below the other points: these data were obtained with a new electrode membrane assembly and its activation was probably incomplete at this time, as confirmed by interpretation of the corresponding impedance spectra. Direct interpretation of the curves shown in Figure 3 could not be achieved because of the low differences in voltage. The kinetic parameters were thereafter estimated from impedance spectra.

3.1. *Theoretical laws*

Transport of protons in the thin electrolyte layer was assumed to be much faster than the charge transfer kinetics, and the concentration ratio $C_{H^+}(0)/C_{H^+}(\infty)$ appearing in Equation (2) applied to the H_2/H^+ system, was therefore taken as one. Values of the parameters given in Table 1 led to a limiting current density, $i_{L,H2}$ of 15 A cm^{-2} for pure hydrogen at 60 °C and 1 Atm, taking into account the vapour pressure at this temperature (0.197 Atm). The current density delivered by the fuel cell was typically below 0.4 A cm^{-2}, far below the limiting cd, which shows the little significant control by diffusion-convection except with the highest dilution of hydrogen.

Tafel slopes for hydrogen oxidation and evolution, b_{T,H_2} and b_{T,H^+} respectively, were taken at $RT/(2F)$ as in Tafel–Volmer mechanism, which has been considered in previous investigations [14, 15]. This corresponds to 33 mV/decade at 60 °C. The following expression for the anode current density was then deduced:

$$i = \frac{\frac{1}{m_{H_2}}\exp\left(\frac{\eta_a}{b_{T,H_2}}\right) - \exp\left(-\frac{\eta_a}{b_{T,H^+}}\right)}{\frac{1}{i_{0,H_2}} + \frac{1}{2FC_{H_2}(\infty)}\left(\frac{\delta_1}{m_{H_2}D_{H_2,\text{eff},1}} + \frac{\delta_2}{m_{H_2}D_{H_2,\text{eff},2}} + \frac{\delta_N}{\gamma D_{H_2,N}}\right)\exp\left(\frac{\eta_a}{b_{T,H_2}}\right)} \tag{7}$$

The charge transfer resistance at the anode was deduced by derivation of Equation (7) regardless of the concentration ratio as follows:

$$\frac{1}{r_{ct,a}} = i_{0,H_2}\left[\frac{1}{b_{T,H_2}}\frac{C_{H_2}(0)}{C_{H_2}(\infty)}\exp\left(\frac{\eta_a}{b_{T,H_2}}\right) + \frac{1}{b_{T,H^+}}\exp\left(-\frac{\eta_a}{b_{T,H^+}}\right)\right] \tag{8}$$

3.2. *Results*

The pseudocapacitance of the anode was found to range from 0.02 to 0.1 S cm^{-2} $s^{0.8}$. In spite of appreciable scatter, Q_a decreased slightly with the current density below 0.2 A cm^{-2}, then remained fairly constant over this limit. The charge transfer resistance decreased regularly with the current density depending on the hydrogen dilution (Figure 4): this dependence showed that for the present work, the high frequency feature could not be ascribed to the distribution of ohmic resistance due to uneven hydration of the MEA, but to hydrogen oxidation, as assumed above.

From the experimental values of charge transfer resistance and current density, the corresponding values for the overpotential were calculated together with the exchange current density by fitting, depending on the hydrogen content in the inlet gas. The fitted variations of $r_{ct,a}$ with i represented the experimental data well, as shown in Figure 4. The exchange current density increased regularly with the hydrogen content in the inlet gas, passing from 86 mA cm^{-2} at 20% H_2 to 314 mA cm^{-2} with pure hydrogen (Table 2).

The exchange current density obeys a power law of $C_{H_2}(\infty)$ with exponent near 0.72: the values obtained with a reduced number of data is in acceptable agreement with the theoretical value of 0.5 deduced from the oxidation mechanism, and the reaction order reported by [14] at 0.42.

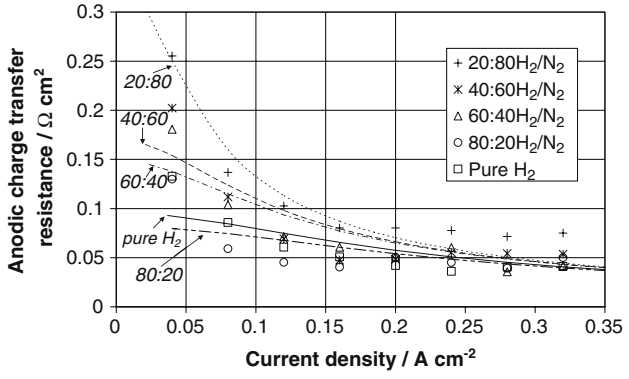

Fig. 4. Anodic charge transfer resistance: experimental values (symbols) and Butler–Volmer law (lines).

Table 2. Exchange current densities of hydrogen oxidation determined from impedance measurements at 60 °C, 1 Atm.

H_2/N_2	i_{0,H_2}/mA cm^{-2} (geometric area)	i_{0,H_2}/mA cm^{-2} (actual area)
20:80	86	0.4
40:60	176	0.9
60:40	201	1.0
80:20	366	1.8
Pure H_2	314	1.6

Air was fed to the cathode

The exchange current density was expressed on the basis of the actual area of the catalyst clusters (Table 2), and the values obtained, of the order of 1 mA cm^{-2}, are in good agreement with data obtained for H_2 oxidation on plate Pt surfaces [15, 16] or for its evolution [17, 18].

The exchange current density for hydrogen oxidation was also determined by feeding the two compartments of the cell with pure hydrogen and measuring the cell impedance at equilibrium. At equilibrium Equation (8) is no longer valid and the usual Butler–Volmer equation to be considered, reduces to:

$$r_{ct,a} = \frac{RT}{2Fi_{0,H_2}} \tag{9}$$

Use of equation 7 for the current density allowed prediction of the variations of the anode overpotential with the delivered current density (Figure 5).

In most cases, the anode overpotential is below 50 mV, confirming the second-order significance of this contribution in the overall voltage balance. Moreover, the difference in η_a calculated for pure hydrogen and 20% H_2 was below 20 mV, which explains that the voltage-current variations reported in Figure 3 were affected little by the dilution factor. However, although moderate, the anode response has to be taken into account in the interpretation of the impedance spectra.

4. Cathodic reduction of oxygen

Kinetic parameters were deduced from the measurements using two methods. First, cathode overpotentials were deduced from the steady measurements presented in section 3, and another series with diluted oxygen at the cathode and pure hydrogen in the other side. Secondly, impedance measurements carried out with pure hydrogen and diluted oxygen, were treated as for investigation with 5 diluted hydrogen.

4.1. *Theoretical laws*

The cell voltage V is linked to the reversible voltage of the cell and the various voltage losses:

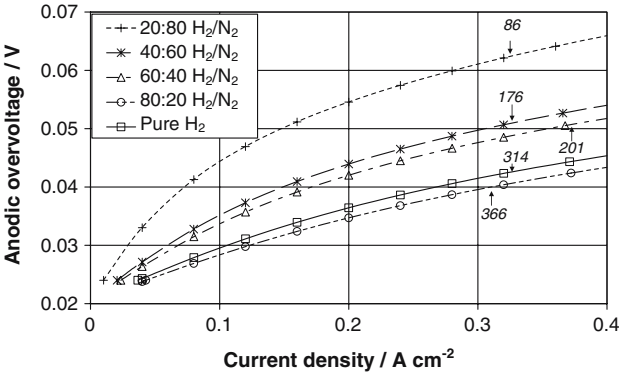

Fig. 5. Anodic overvoltage for all hydrogen dilutions. Corresponding values of exchange current densities are given.

$$U_{\text{rev}} = V + \eta_a + |\eta_c| + r_{\text{ohm}} i \quad (10)$$

Steady measurements carried out with diluted oxygen led to (V–i) variations. The ohmic resistance was determined, and the anodic overpotential could be determined as explained above (Figure 5). The reversible voltage was calculated using the following Nernst law, which was employed in previous investigations [19, 20]:

$$U_{\text{rev}} = \frac{70650 + 8.0\ln(T) - 92.84T}{8.368F} + \frac{RT}{4F}\ln(P_{O_2}) + \frac{RT}{2F}\ln(P_{H_2}) \quad (11)$$

T is in Kelvin and pressures in Atm

The limiting current density estimated using the parameters values of Table 1 attained 9.4 A cm^{-2} for pure oxygen in the dry gas, and 1.97 A cm^{-2} for air. In the latter case, mass transfer partly controlled the overall reduction, as confirmed by the low frequency loop of the impedance spectra.

Cathodic reduction of oxygen can be considered as irreversible. Introducing b_{T,O_2} as the Tafel parameter of the reduction yielded an expression for the absolute current density (noted i in this section):

$$i = i_{0,O_2}\frac{C_{O_2}(0)}{C_{O_2}(\infty)}\exp\left(-\frac{\eta_c}{b_{T,O_2}}\right) \quad (12)$$

The cathode overpotential was then deduced from the current density:

$$|\eta_c| = b_{T,O_2}\ln\left(\frac{i}{C_{O_2}(0)/C_{O_2}(\infty)}\right) - b_{T,O_2}\ln i_{0,O_2} \quad (13)$$

in which the concentration ratio is given by Equation (5)

The charge transfer resistance at the anode was deduced by derivation of Equation (12):

$$r_{ct,O_2} = \frac{b_{T,O_2}}{i} \quad (14)$$

4.2. *Measurements at steady state*

For both series of data, the absolute overpotential of the cathode calculated from the data varied from 400 to 580 mV, depending on the current density. Plotting $|\eta_c|$ vs. $\log\left(\frac{i}{C_{O_2}(0)/C_{O_2}(\infty)}\right)$ led to linear variations (Figure 6) in agreement with Equation (13).

Because the first series corresponds to the same oxygen content and similar water management, all data were expected to merge into one line. The deviations observed in Figure 6(a) may stem from the numerous numerical treatments carried out for estimation of the cathode overpotential. As shown in Table 3a, the Tafel slope varied from 130 to 139 mV/decade with diluted hydrogen whereas it attained 161 mV/decade with pure hydrogen. Data obtained with diluted oxygen also led to linear variations (Figure 6(b)), with Tafel plots ranging from 124 to 151 mV/decade except for pure oxygen (Table 3(b)).

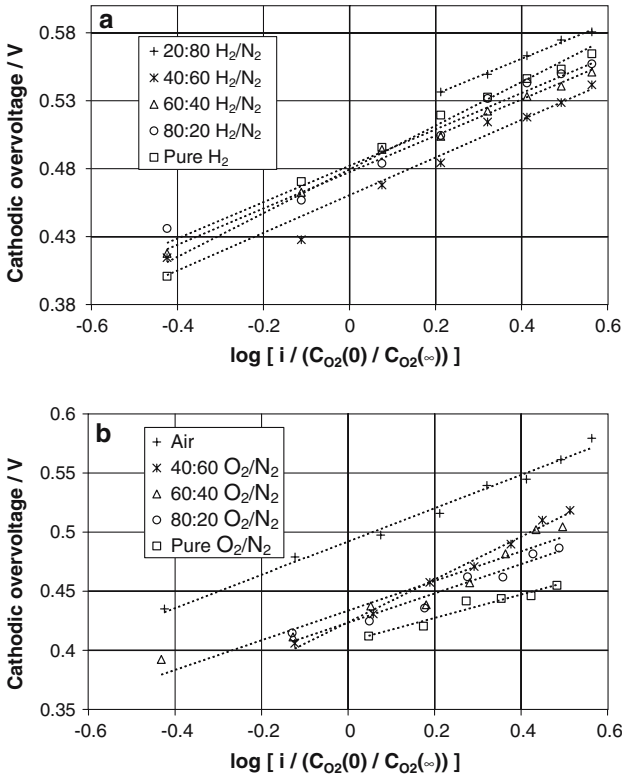

Fig. 6. Tafel plots of cathodic overpotential vs. concentration-corrected current density. (a) for all hydrogen dilutions. (b) for all oxygen dilutions.

This result is in perfect agreement with the conclusions of numerous investigations carried out at moderate/high current densities. The slope at 120 mV/decade at ambient temperature is usually ascribed to the Langmuir isotherm of oxygen adsorption on Pt surfaces, corresponding to a rate-controlling step involving one

Table 3. (a) Exchange current densities of oxygen reduction determined from impedance measurements at 60 °C, 1 Atm.Air was fed to the cathode; (b) Pure hydrogen was fed to the anode

	Tafel slope/ mV dec^{-1}	i_{0,H_2}/mA cm^{-2} (geometric area)	i_{0,H_2}/mA cm^{-2} (actual area)
(a) H_2/N_2			
20:80	130	1.4×10^{-4}	0.7×10^{-6}
40:60	139	3.2×10^{-4}	1.6×10^{-6}
60:40	134	2.4×10^{-4}	1.2×10^{-6}
80:20	134	2.2×10^{-4}	1.1×10^{-6}
Pure H_2	161	2.3×10^{-4}	1.2×10^{-6}
(b) O_2/N_2			
21:79 (air)	141	1.9×10^{-4}	0.94×10^{-6}
40:60	151	6.2×10^{-4}	3.1×10^{-6}
60:40	125	5.2×10^{-4}	2.6×10^{-6}
80:20	124	6.2×10^{-4}	3.1×10^{-6}
Pure O_2	99	8.2×10^{-4}	4.1×10^{-6}

electron: applying the data reported in [21, 22] to the actual temperature led to a slope near 132 mV/decade.

The exchange current density of air oxygen reduction based on the geometrical area, was in the range 1.4–3.2 $\times$ 10^{-4} A cm^{-2}, corresponding to 0.7–1.6 μA cm^{-2} considering the catalyst active area. Increasing the oxygen content in the gas fed to the cathode compartment resulted in reduction in $|\eta_c|$ by 50 mV (Figure 6(b)), and to appreciable increase in exchange current densities, up to 8.2 $\times$ 10^{-4} cm^{-2} with pure H_2–O_2 (Table 3(b)). The order of magnitude for i_{0,O_2} is perfectly consistent with published values [23, 24]. Finally, from the second series of experiments, the exchange current density was shown to vary with the oxygen concentration in the gas phase to the power 0.85, in good agreement with the first-order process.

4.3. *Results from interpretation of impedance spectra*

Impedance spectra recorded with diluted oxygen at the cathode and pure hydrogen at the anode side were treated as explained above. The exponent of the constant phase element slightly decreased with current density, from 0.8 to 0.7 for the highest cd. The pseudocapacitance of the anode was found to range from 0.04 to 0.15 S cm^{-2} $s^{\alpha\ c}$.

Because of the irreversibility of the reduction, the values of the charge transfer resistance could not be used to calculate the exchange current density, and only the Tafel slope could be obtained. As expected from Equation (14), the charge transfer resistance varied linearly with the reciprocal of the current density depending on the hydrogen dilution (Figure 7).

The slopes of the straight lines yielded Tafel slopes, ranging from 116 to 132 mV/decade for the four O_2–N_2 mixtures considered. Use of pure oxygen resulted in a Tafel slope near 100 mV/decade. However, fitting the data with pure O_2 omitting the point obtained at 40 mA cm^{-2} yielded a slope near 120 mV/decade.

The intercept of the linear variation at infinite current density should result in a zero charge transfer resistance. Examination of Figure 7 indicates appreciable values of $r_{ct,c}$ for nil values of $(1/i)$. The observed discrepancy with the theory might be due to the fact that the measured resistance could contain a part of the diffusion resistance, due to partial overlapping of the two features, and a term corresponding to the ratio of the surface-over-bulk concentrations should be added. However, use of the intercept value for further interpretation cannot be carried out without restrictive assumptions [25], and this point was not treated here.

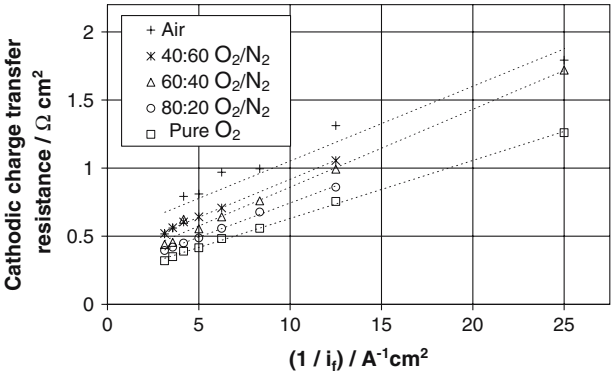

Fig. 7. Tafel plots of cathodic charge transfer resistance for all oxygen dilutions.

5. Conclusion and significance

The separate responses of the electrodes of a PEMFC were observed for operation of the fuel cell at ambient pressure, without a reference electrode. For this purpose, magnification of electrode responses was achieved by feeding the cell either with diluted hydrogen – for anode investigation – or with diluted oxygen at the cathode, for well-controlled water management of the cell. Steady measurements of the voltage at fixed current density together with impedance spectroscopy allowed the kinetics of both reactions to be investigated. Hydrogen kinetics at the conventional anode of the fuel cell could be described by the Tafel–Volmer mechanism, and the anode overpotential varied from 20 to 50 mV depending on the dilution factor and the current density. Moreover, the exchange current density and the Tafel slope for O_2 reduction were found to be in perfect agreement with published results both at flat Pt surfaces and at the surface of a FC cathode.

Acknowledgements

The authors are indebted to Region Lorraine and CNRS for funding facilities – through PACEM "PRI" – and the Ph.D. grant allocated to M.B.

References

1. G. Li and P.G. Pickup, *Electrochim. Acta* **49** (2004) 4119.
2. Z. Liu, J.S. Wainright, W. Huang and R.F. Savinell, *Electrochim. Acta* **49** (2004) 923.
3. Z. Siroma, R. Kakitsubo, N. Fujiwara, T. Ioroi, S.I. Yamazaki and K. Yasuda, *J. Power Sources* **156** (2006) 284.
4. H. Kuhn, B. Andreaus, A. Wokaun and G.G. Scherer, *Electrochim. Acta* **51** (2005) 1622.
5. T.J.P. Freire and E.R. Gonzales, *J. Electroanal. Chem.* **503** (2001) 57.
6. V.A. Paganin, C.L.F. Oliveira, E.A. Ticianelli, T.E. Springer and E.R. Gonzales, *Electrochim. Acta* **43** (1998) 3761.
7. M. Boillot, C. Bonnet, N. Jatroudakis, P. Carré, S. Didierjean and F. Lapicque, *Fuel Cells* **6** (2005) 31.
8. M. Sluyters-Rehbach, *Pure Appl. Chem.* **66** (1994) 1831.
9. B.A. Boukamp, *Solid State Ionics* **20** (1986) 31.
10. T.E. Springer, T.A. Zawodzinski, M.S. Wilson and S. Gottesfeld, *J. Electrochem. Soc.* **143** (1996) 587.
11. P. Gode, F. Jaouen, G. Lindbergh, A. Lundblad and G. Sundholm, *Electrochim. Acta* **48** (2003) 4175.

12. D.M. Bernardi and M.W. Verbrugge, *AIChE J.* **37** (1991) 1151.
13. M. Ciureanu and R. Roberge, *J. Phys. Chem. B* **105** (2001) 3531.
14. J. Vermeijlen, L.J.J. Janssen and G.J. Visser, *J. Appl. Electrochem.* **27** (1997) 497.
15. B.E. Conway and B.V. Tilak, *Electrochim. Acta* **47** (2002) 3571.
16. R.M.Q. Mello and E.A. Ticianelli, *Electrochim. Acta* **42** (1997) 1031.
17. B.E. Conway and L. Bai, *J. Electroanal. Chem.* **198** (1986) 149.
18. B.V. Tilak and C.P. Chen, *J. Appl. Electrochem.* **23** (1993) 631.
19. A. Parthasarathy, S. Srinivasan, A.J. Appleby and C.R. Martin, *J. Electrochem. Soc.* **139** (1992) 2530.
20. V.I. Basura, P.D. Beattie and S. Holdcroft, *J. Electroanal. Chem.* **458** (1998) 1.
21. D.B. Sepa and M.V. Vojnovic, *Electrochim. Acta* **25** (1980) 1491.
22. A. Damjanovic, D.B. Sepa and M.J. Vojnovic, *Electrochim. Acta* **24** (1979) 887.
23. L. Zhang, C. Ma and S. Mukerjee, *J. Electroanal. Chem.* **568** (2004) 273.
24. O. Antoine, Y. Bultel and R. Durand, *J. Electroanal. Chem.* **499** (2001) 85.
25. Boillot M., Validation expérimentale d'outils de modélisation d'une pile à combustible de type PEM, Ph.D dissertation, (INPL, Nancy 2005).